Pairing correlations in the attractive Hubbard model on chains, ladders, and squares

M. Guerrero, G. Ortiz, and J. E. Gubernatis

Theoretical Division, Los Alamos National Laboratory, Los Alamos, New Mexico 87444

(Received 7 December 1999)

We report the results of zero-temperature quantum Monte Carlo simulations and zero-temperature mean-field calculations of the attractive Hubbard model on chains, ladders, and square lattices. We investigated the predictability of the BCS approximation, the dimensional crossover of the pairing correlation function from one to two dimensions as a function of the ladder width, and the scaling of these correlations to the thermodynamic limit of the two-dimensional model. We found that the BCS wave function is quantitatively correct only for small values of U/t. For the system sizes, electron fillings, and interaction strengths studied, we never saw the dimensional crossover. In general, our ability to achieve the dimensional crossover and accurate scaling to the thermodynamic limit was limited by the size of the systems we could simulate. For these sizes, although we saw the necessary signature of off-diagonal long-range order, the properties of the model did not vary monotonically with increasing system size because of shell effects. We contrast this situation with the dimensional crossover and scaling to the thermodynamic limit of the Ising model.

I. INTRODUCTION

We report the results of zero-temperature quantum Monte Carlo (QMC) simulations and zero-temperature mean-field calculations of the attractive Hubbard model on chains, ladders, and square lattices. We investigated the predictability of the BCS approximation, the dimensional crossover of pairing correlations from one to two dimensions as a function of the ladder width, and the scaling of these correlations to the thermodynamic limit of the two-dimensional model. We found that the BCS wave function is quantitatively correct only for weak attractive interactions. For the system sizes, electron fillings, and interaction strengths studied, we never saw the dimensional crossover, and we were unable to scale the pairing correlations on finite-size square lattices to those on infinitely sized ones. In general, our ability to achieve the dimensional crossover and the proper scaling to the thermodynamic limit was limited by the size of the systems we could simulate. For these sizes, although we saw the necessary signature of off-diagonal long-range order (ODLRO), the properties of the model did not vary monotonically with increasing system size because of shell effects.

The BCS wave function occupies a deservedly prominent place in the theory of superconductivity. For traditional superconductors, the electron-phonon interaction induces an attractive interaction between pairs of electrons that is well described by the reduced BCS Hamiltonian[1]

$$H = \sum_{\mathbf{k}\sigma} \epsilon_{\mathbf{k}} n_{\mathbf{k},\sigma} - \sum_{\mathbf{k},\mathbf{k}'} V_{\mathbf{k},\mathbf{k}'} c^{\dagger}_{\mathbf{k},\uparrow} c^{\dagger}_{-\mathbf{k},\downarrow} c_{-\mathbf{k}',\downarrow} c_{\mathbf{k}',\uparrow}, \quad (1)$$

and the BCS wave function

$$|\text{BCS}\rangle = \prod_{\mathbf{k}} (u_{\mathbf{k}} + v_{\mathbf{k}} c^{\dagger}_{\mathbf{k},\uparrow} c^{\dagger}_{-\mathbf{k},\downarrow})|0\rangle \quad (2)$$

provides an excellent approximation to the eigenstates of this Hamiltonian. In fact, under a number of circumstances, it is the exact solution in the thermodynamic limit.[2]

Characteristic of BCS-like superconductors is the large number of Cooper pairs inside the volume defined by the coherence length a_0 of a pair. In high-temperature (cuprate) superconductors, as well as several other classes of much lower temperature superconductors, including doped cuprate ladders,[4] the coherence length is comparatively small. For these materials, one often proposes the attractive Hubbard model

$$H = -t \sum_{\langle ij \rangle, \sigma} (c^{\dagger}_{i,\sigma} c_{j,\sigma} + c^{\dagger}_{j,\sigma} c_{i,\sigma}) - U \sum_{i} n_{i,\uparrow} n_{i,\downarrow}, \quad (3)$$

where $U > 0$, as a counterpart to the BCS reduced Hamiltonian. Indeed, for any allowable electron filling, two electrons are energetically favored to pair onto a lattice site, thus giving them a seemingly very short coherence length. For dimensions of two and higher, the ground-state possesses s-wave ODLRO in the thermodynamic limit over certain ranges of electron fillings if the lattice is bipartite and the number of A sites does not equal the number of B sites, a condition not satisfied, for example, by a square lattice.[3]

In this work we studied the attractive Hubbard model on chains, ladders, and squares, using an exact QMC method. The attractive Hubbard model has no fermion sign problem so it is relatively easy to study by QMC simulations. One goal was to observe the dimensional crossover of the superconducting pairing correlation functions from the well-known power-law behavior in one dimension to ODLRO in two dimensions. We studied mostly the quarter filled system and compared our results with the predictions of the BCS approximation. We tried to establish the range of validity of this approximation, and for the square lattices we tried to investigate both the weak and strong-coupling regimes to assess the validity of the argument of Nozières and Schmitt-Rink[5] regarding the smooth crossover from one regime to the other.

Nozières and Schmitt-Rink[5] studied the transition from weak- to strong-coupling superconductivity in an attractive continuum fermion model

$$H = \sum_{\mathbf{k},\sigma} \frac{k^2}{2m} n_{\mathbf{k},\sigma}$$

$$- \sum_{\mathbf{k},\mathbf{k}',\mathbf{q}} V_{\mathbf{k},\mathbf{k}'} c^{\dagger}_{\mathbf{k}+\mathbf{q}/2,\uparrow} c^{\dagger}_{-\mathbf{k}+\mathbf{q}/2,\downarrow} c_{-\mathbf{k}'+\mathbf{q}/2,\downarrow} c_{\mathbf{k}'+\mathbf{q}/2,\uparrow},$$

$$(4)$$

and the attractive lattice Hamiltonian (3). For both models, they argued that the BCS wave function is a good approximation in the weak- and strong-coupling limits. In the continuum model, weak coupling corresponds to carrier densitites $\langle n \rangle$ satisfying $\langle n \rangle a_0 \gg 1$, and strong coupling satisfying the opposite limit. For the lattice model, coupling strength corresponds to the relative size of the interaction strength U and the noninteracting bandwidth W: Strong coupling is $U \gg W$ and weak coupling is $U \ll W$. Further, they argued that this approximation interpolates smoothly and accurately between these limits, a remarkable fact because of the distinctly different physics occurring at these limits: For weak coupling, Cooper pairs form according to the usual BCS picture; for strong coupling, (Schafroth) pairs are hard-core bosons which may Bose condense.

We found the weak-coupling regime for a quarter-filled system, i.e., $\langle n \rangle = 1/2$, on a square lattice is limited to values of U/t satisfying $0 \lesssim U/t \lesssim 1$. For larger values of U/t, significant disagreements in the values of on-site s-wave pairing correlations existed between the results of the simulations and the predictions of the BCS approximation. These disagreements remained for values of U/t as large as 8, which is as large as we could push our simulations, and suggest the strong-coupling regime, if the arguments of Nozières and Schmitt-Rink are correct, lies well beyond $U/t = 8$. (With our numerical technique we can only accurately simulate values of U comparable to the size of W.)

We comment that in the strong-coupling limit ($U/t \gg 1$ and with any band filling of an even number of fermions), the attractive Hubbard model, up to second order in degenerate perturbation theory, maps to an interacting hard-core boson system in the subspace of doubly occupied and empty sites.[6] These bosons hop to nearest neighbors with an effective amplitude $-2t^2/U$ and interact with a nearest-neighbor repulsion $2t^2/U$. However, the BCS wave function is the exact eigenstate of this effective problem only in the completely empty and completely filled lattice cases (see Appendix A). From our analysis we are unable to say whether away from the extreme cases the BCS fixed point is the correct strong-coupling limit. The BCS fixed point can still be the correct one and large quantitative differences can exist.

Our main object of study was pairing correlation functions. We found that the distance dependent pairing properties of the model on a square lattice did not vary monotonically as we systematically expanded its size, and we were unable to obtain a very accurate estimate of the order parameter in the thermodynamic limit, even though it is clear from the calculations that the system has ODLRO in that limit. This shortcoming contrasts a much earlier zero-temperature QMC study[7] that claimed to do such an extrapolation on the integrated pairing correlation function and obtained a value for the order parameter consistent with our results. Our computed results for the long-range spatial dependence of the

s-wave pairing correlations for a long chain compared very favorably with the Bethe ansatz predictions for a chain in the thermodynamic limit. Systematically coupling these long chains did not produce a monotonic variation in these correlations, and computational costs forced us to limit our study to a $L \times 4$ systems with $L \sim 50$. We believe the irregular variations in the properties of the rectangular and square structures are consequences of shell effects characteristic of finite-sized systems of fermions. We remark that increasing the value of U/t reduces the shell effects as one would expect. These finite-size shell effects prevented us from observing the crossover to the two-dimensional behavior in the correlation functions. Wider systems or larger values of the interactions are needed to observe such crossover.

In the next section we summarize several useful exact properties of the attractive Hubbard model in two dimensions, and then in Sec. III, we summarize our numerical approach. In Sec. IV we present our main results, and in the final section, Sec. V, we will discuss the implications of our results and the effects of finite size on other simulations of interacting electron systems.

II. ATTRACTIVE HUBBARD MODEL

A number of exact statements can be made about the properties of the attractive Hubbard model at zero-temperature. In one dimension the most important statements for present purposes are the absence of any long-range order[8] and the inverse power-law form for the pairing correlation function at large distances between pairs.[9] In this section we will focus on those statements that are at least true for ground-state properties in two dimensions. Most are, in fact, true for any dimension. Most assume a bipartite lattice. Unfortunately, we are unaware of any exact results assuring the model on a square lattice has ODLRO. The Mermin-Wagner theorem[10] only assures that long-range order (LRO) cannot exist in two dimensions at finite temperature. We are also unaware of any pertinent theorems regarding the attractive Hubbard model on ladder structures.

Perhaps the most fundamental theorem says the ground state for an even number of electrons is a nondegenerate singlet for every electron filling.[11] On the other hand, the most useful property of the model is its mapping for any electron filling onto a half filled repulsive Hubbard model in a magnetic field.[12] Charge and pairing operators map into pseudospin operators and vice versa. A specific version of this mapping maps staggered components of the pseudospin operators in the half filled repulsive model into charge and pairing operators in the attractive half filled model.[13]

At half filling, on-site s-wave ODLRO exists in the attractive Hubbard model if and only if a charge-density wave (CDW) LRO exists.[14] It is generally accepted that the ground state of the half filled, two-dimensional, repulsive model is one of antiferromagnetic (AF) LRO. Because longitudinal pseudospin maps to charge, and transverse pseudospin to pairing, the acceptance of AF LRO for the half filled repulsive model seems sufficient to establish on-site s-wave ODLRO and CDW LRO as ground states of the half filled attractive model. Indeed numerical studies support this conclusion.[7]

Another theorem states if the charge spectrum is gapped

in either the repulsive or attractive models, then there can be no on-site s-wave ODLRO.[15] It is generally accepted that the ground state of the half filled, two-dimensional repulsive model has a charge gap. This presence implies a spin gap for the ground state of the half filled, two-dimensional attractive model. Thus the theorem does not violate the inference of ODLRO in the attractive model at half filling.

In this paper we are exclusively interested in the properties of the attractive model away from half filling. Here a theorem states that on-site s-wave ODLRO exists if and only if extended s-wave ODLRO exists.[16] Noteworthy is that this theorem also states that the magnitude of the order parameter for the extended s-wave state vanishes as half filling is approached, making the doped case essentially different in character from the half filled case. In particular, if $\langle \Delta_s \rangle$ is the expectation value of the on-site s-wave order parameter and $\langle \Delta_{s*} \rangle$ is that of extended s-wave, then

$$\langle \Delta_{s*} \rangle = \frac{-U - 2\mu}{t} \langle \Delta_s \rangle, \tag{5}$$

where μ is the chemical potential. At half filling, because of particle-hole symmetry, $2\mu = -U$. Accordingly, at half filling $\langle \Delta_{s*} \rangle = 0$. We comment that this relation between the extended s-wave order parameter and the on-site (isotropic) s-wave order parameters depends on the hopping integral being isotropic. If one were to set, for example, $t_x = t$ and $t_y = -t$, the $d_{x^2-y^2}$-wave order parameter would appear on the left-hand side of Eq. (5). In the isotropic hopping case we did not see any significant signal of d-wave pairing. In Appendix A, we prove the equivalent theorem for the BCS approximation.

Ground-state numerical studies away from half filling see a necessary signature of on-site s-wave ODLRO order.[7] The pair-pair correlation function clearly does not vanish when the pairs are well separated. To establish ODLRO one also needs to show that this correlation also does not vanish in the thermodynamic limit. Establishing this for the two-dimensional attractive model was one of our goals. To achieve this objective we used an exact QMC method, that is, a method with no sign problem. We now summarize this method.

III. NUMERICAL APPROACH

The details of our numerical approach are the same as those for the constrained-path Monte Carlo (CPMC) method[17] except we have no constraint because the simulations have no sign problem. Because of this, apart from statistical error, the method is exact. Briefly the strategy of our approach is as follows:

Starting with some trial state $|\psi_T\rangle$, we project out the ground state by iterating

$$|\psi'\rangle = e^{-\Delta\tau(H - E_T)}|\psi\rangle, \tag{6}$$

where E_T is some guess of the ground-state energy. Purposely $\Delta\tau$ is a small parameter so for $H = T + V$ we can write

$$e^{-\Delta\tau H} \approx e^{-\Delta\tau T/2} e^{-\Delta\tau V} e^{-\Delta\tau T/2}, \tag{7}$$

where T and V are the kinetic and potential energies. We used values of $\Delta\tau$ ranging from 0.03 to 0.05.

For the study at hand, the initial state $|\psi_T\rangle$ is the direct product of two spin Slater determinants, i.e.,

$$|\psi_T\rangle = \prod_\sigma |\phi_T^\sigma\rangle. \tag{8}$$

Because the kinetic energy is a quadratic form in the creation and destruction operators for each spin, the action of its exponential on the trial state is simply to transform one direct product of Slater determinants into another. While the potential energy is not a quadratic form in the creation and destruction operators, its exponential is replaced by the sum of exponentials of such forms via the discrete Hubbard-Stratonovich transformation

$$e^{\Delta\tau U n_{i,\sigma} n_{i,-\sigma}} = \frac{1}{2} e^{-(1/2)\Delta\tau U} \sum_{x=\pm 1} e^{-x\Delta\tau J(n_{i,\sigma} + n_{i,-\sigma} - 1)}$$
$$\times e^{(1/2)\Delta\tau U(n_{i,\sigma} + n_{i,-\sigma})} \tag{9}$$

provided $U \geq 0$ and $\cosh\Delta\tau J = e^{\Delta\tau U/2}$. Accordingly we re-express the iteration step as

$$\prod_\sigma |\phi'_\sigma\rangle = \int d\vec{x} P(\vec{x}) \prod_\sigma B_\sigma(\vec{x})|\phi_\sigma\rangle, \tag{10}$$

where $\vec{x} = (x_1, x_2, \ldots, x_N)$ is the set of Hubbard-Stratonovich fields (one for each lattice site), N is the number of lattice sites, $P(\vec{x}) = (\frac{1}{2})^N$ is the probability distribution for these fields, and $B_\sigma(\vec{x})$ is an operator function of these fields formed from the product of the exponentials of the kinetic and potential energies.

Upon examination, one sees that $B_\sigma(\vec{x}) = B_{-\sigma}(\vec{x}) \equiv B(\vec{x})$. This equivalence means the equivalence of the propagators for the separate spin components of the initial state. If these components are identical, i.e., if $|\phi_T^\sigma\rangle = |\phi_T^{-\sigma}\rangle \equiv |\phi_T\rangle$, then only one component needs to be propagated:

$$|\phi'\rangle = \int d\vec{x} P(\vec{x}) B(\vec{x})|\phi\rangle, \tag{11}$$

but more importantly, the overlap of the initial state with the current state $\langle \psi'|\psi_T\rangle = \langle \phi'|\phi_T\rangle^2$ and thus is always positive. This positivity is sufficient to eliminate the sign problem.

The Monte Carlo method is used to perform the multidimensional integration over the Hubbard-Stratonovich fields. It does so by generating a set of random walkers initialized by replicating $|\psi_T\rangle$ many times. Each walker is then propagated independently by sampling a $\vec{x}$ from $P(\vec{x})$ and propagating it with $B(\vec{x})$. After the propagation has "equilibrated," the sum over the walkers provides an estimate of the ground-state wave function $|\psi_0\rangle$.

In practice, we performed an importance-sampled random walk, obtained by defining for each Slater determinant $|\phi\rangle$ another one $|\bar{\phi}\rangle$ via

$$|\bar{\phi}\rangle = \langle \phi_T|\phi\rangle|\phi\rangle, \tag{12}$$

and using the transformed iterative equation

$$|\tilde{\phi}'\rangle = \int d\vec{x}\,\tilde{P}(\vec{x})B(\vec{x})|\tilde{\phi}\rangle. \qquad (13)$$

In this equation

$$\tilde{P}(\vec{x}) = P(\vec{x})\frac{\langle\phi_T|\phi'\rangle}{\langle\phi_T|\phi\rangle}. \qquad (14)$$

Thus importance sampling changes the probability distribution of the Hubbard-Stratonovich fields, biasing it towards the generation of states with large overlap with the initial state. The branching nature of the random walk is the same as described for the CPMC method and will not be discussed here. It is a necessary procedure for controlling the variance of the computed results.

We used two different estimators for the expectation values of some observable $\mathcal{O}$. One is the mixed estimator

$$\langle\mathcal{O}\rangle_{\text{mixed}} = \frac{\langle\psi_T|\mathcal{O}|\psi_0\rangle}{\langle\psi_T|\psi_0\rangle}, \qquad (15)$$

and the other is the back-propagated estimator

$$\langle\mathcal{O}\rangle_{\text{bp}} = \frac{\langle\psi_T|e^{-l\Delta\tau H}\mathcal{O}|\psi_0\rangle}{\langle\psi_T|e^{-l\Delta\tau H}|\psi_0\rangle}, \qquad (16)$$

where $|\psi_0\rangle$ is the QMC estimate of the ground state and l is typically in the range of 20 to 40. For observables that commute with the Hamiltonian, the mixed estimator is a very accurate one and converges to the exact answer as $|\psi_0\rangle$ converges to the exact ground state. For observables that do not commute with the Hamiltonian, like correlation functions, the back-propagated estimator has been found to give very accurate estimates of ground-state properties. Significant differences between the predictions of these two estimators often exist.

We remark that we could have projected to the ground state using the BCS wave function as our starting point.[18] This wave function is not normally represented as a direct product of two spin Slater determinants, but by a trick proposed by Yokayama and Shiba,[19] one can re-express it as a single Slater determinant. In this new representation, one can then show that there is still no sign problem, but that the computational cost of working with this wave function is at least a factor of 4 more. Since no statistically significant differences in computed results occur, we almost exclusively used the computationally more efficient direct product of free-electron wave functions for $|\psi_T\rangle$. Additionally, most of our calculations were done for closed-shell electron fillings, i.e., nondegenerate electron fillings in the noninteracting problem. For these fillings and for the same amount of computing time, the statistical error of our expectation values is considerably smaller than that of our expectation values at open-shell fillings (which can be easily handled when the BCS wave function is used as constraint[18]).

We also remark that the standard auxiliary-field projector Monte Carlo method also has no sign problem for the attractive Hubbard model. Although only a few comparisons exist, we are unaware of any statistically significant differences between results from that method and results from the one used here. If both are exact procedures, then, of course, there should not be any. The estimators used in the two methods

TABLE I. Summary of relevant parameters of the QMC simulations. Shown are the systems sizes, the electron fillings $\langle n\rangle$, and the exponent β of the power-law decay for $U/t = 2$. For two- and three-legged ladders, where there is a double entry, for example, 50×2, the top entry gives the value of β for the top envelope, while the bottom entry is for the bottom envelope. In one dimension the fillings are always $\langle n\rangle = 1/2 + 1/L$.

System size	$\langle n\rangle$	β
34×1	0.53	0.88(9)
42×1	0.52	0.82(6)
50×1	0.52	0.86(4)
66×1	0.52	0.79(3)
50×1	0.52	0.86(4)
50×2	0.50	1.07(3)
		0.87(2)
50×3	0.51	1.32(4)
		0.95(3)
50×4	0.51	0.68(5)
6×6	0.5	
8×8	0.5	
10×10	0.5	
12×12	0.51	
14×14	0.5	
16×8	0.45	

however are different as the auxiliary-field projector method uses a different back-propagation estimator for all observables.

IV. RESULTS

In sequence we will now report and discuss results for the attractive Hubbard model on chains, squares, and ladders. In each case we will comment on the predictions of the BCS approximation relative to the predictions of the QMC simulations. For chains we will also comment on supportive calculations we performed using the density-matrix renormalization-group (DMRG) method.[20] Included in a separate subsection is a discussion on the specific issue of dimensional crossover.

Because the variances of our computed results are smaller for closed-shell fillings, we only considered such fillings, and because the shell structure changes with lattice size, as we changed lattice sizes, we could not maintain the electron densities $\langle n\rangle$ at a fixed value. For the results reported here, we fixed the electron density as close as possible to the quarter filled value, that is, to a value of one electron per two lattice sites. The actual fillings for many of the lattices studied are given in Table I. In all cases we had equal numbers of up- and down-spin electrons. In one-dimension we used $\langle n\rangle = 1/2 + 1/L$ which converges to quarter filling as L is increased. We remark that the accuracy of our QMC calculations were benchmarked against those of exact diagonalizations calculations of 4×4 lattices. The QMC results, and in particular those computed by the back-propagation estima-

tors, agreed well within statistical error with those of the more precise method.

A. Chains

For both finite and infinite chain lengths one can obtain the energies of the attractive Hubbard model from its Bethe ansatz solution.[8] Marsiglio and Tanaka,[21,22] for example, have made extensive comparisons of these energies with the predictions of the BCS approximation. Additionally, by computing the Bethe ansatz energies for systems of N_e, N_e-1, and N_e+1 electrons, they also calculated the pair binding energy by evaluating $\Delta_{N_e} = (E_{N_e-1} - 2E_{N_e} + E_{N_e+1})/2$, which in the BCS approximation is the gap Δ.[23] The energy is the least accurate at intermediate coupling strengths at half filling, where the disagreement however is only a few percent, and becomes exact in the weak- and strong-coupling limits at low electron density. In general, the pair binding energy is poorly reproduced, with the disagreement being the least in the dilute electron-density limit. Typically, the BCS wave function overestimates the binding energy. For finite-size systems they also found significant shell effects in the energy as a function of electron density or as a function of chain length in the weak-coupling regime. They did not investigate the pairing correlations.

Exact analysis of the Bethe ansatz solution by Kawakami and Yang[9] showed that in the thermodynamic limit the on-site s-wave pairing correlation function $P_s(R)$ behaves like

$$P_s(R) = \langle \Delta_s^\dagger(R) \Delta_s(0) \rangle \sim \frac{1}{R^\beta} \qquad (17)$$

at large separations R between the pairs. The nonuniversal exponent β is a function of both U/t and the electron filling. (Kawakami and Yang provide a graph giving β for a selection of values of U/t for all fillings between 0 and 1.) Because the BCS approximation always predicts ODLRO, its predictions for the behavior of pairing correlation functions is qualitatively incorrect.

We computed the on-site s-wave pairing function in several different ways. In the QMC simulations, we used periodic boundary conditions, took

$$\Delta_s(i) = c_{i,\downarrow} c_{i,\uparrow}, \qquad (18)$$

and then calculated

$$P_s(R) = \frac{1}{L} \sum_i \langle \Delta_s^\dagger(i+R) \Delta_s(i) \rangle \qquad (19)$$

for each possible value of R by using the back-propagation estimator. In the DMRG calculation, we used open boundary conditions and computed $P_s(R)$ in two different ways. In the first way we computed

$$P_s(R) = \langle \Delta_s^\dagger(i_R+R) \Delta_s(i_R) \rangle \qquad (20)$$

for each value of R relative to some site i_R, which depends on R, chosen to place the pairs as close to the center of the chain as possible. In other words, to avoid edge effects, for a given value of R, we used the sites closest to the center. At the large values of R, the resulting estimate displayed rapid fluctuations that made comparisons with the QMC and Bethe
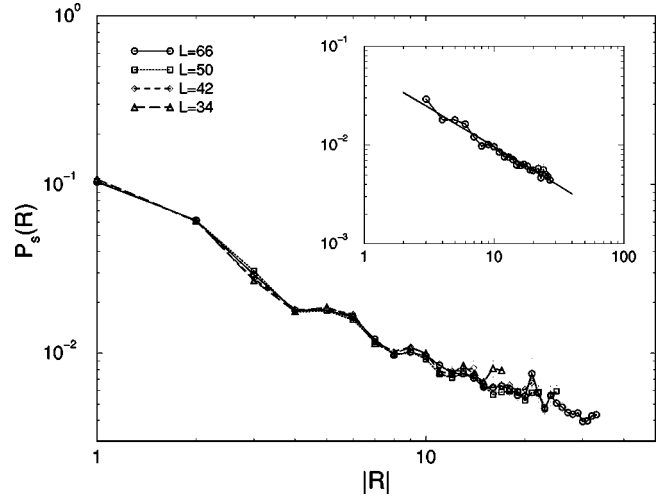

FIG. 1. The QMC on-site s-wave pairing correlation function $P_s(R)$ as a function of the distance $|R|$ between pairs for a $U/t = 2$ chain of different lengths L. The inset shows the fit of results for the $L=66$ chain to the inverse power-law form (17) using a value of $\beta = 0.79$.

ansatz predictions difficult. We found we could smooth out the fluctuations by computing $P_s(R)$ from[24]

$$P_s(R) = \frac{1}{N_p(R)} \sum_{i=1}^{N_p(R)} \langle \Delta_s^\dagger(R) \Delta_s(0) \rangle_i. \qquad (21)$$

Here we sum over all possible pairs of lattice sites separated by the same displacement R and divide this sum by the number $N_p(R)$ of such pairs of sites, which is a function of R. At large values of R, this function was much smoother. More importantly, it compared very well with the QMC results.

In Figs. 1 and 2 we show samples of our results for $U/t = 2$. In Fig. 1, we superimpose several calculations of $P_s(R)$ for different chain lengths L to illustrate that increasing the chain length did not change the pairing correlations at short and intermediate distances. It simply increased the range in distance over which we correctly captured these correlations. We fitted the large distance behavior of the correlation functions to the inverse power-law function (17) and found exponents β consistent with the Bethe ansatz prediction. For example, from Kawakami and Yang's graph, we estimated $\beta = 0.80(2)$. Our fit for the chain of $L=66$, shown in the inset to Fig. 1, predicted $\beta = 0.79(3)$. Exponents for other fits are given in Table I. For long enough chains we obtained close agreement between the value of β obtained by fitting and the value obtained from Kawakami and Yang's graph. In performing the fit we eliminated the short-range behavior and the upturn in the correlations at large distances. This upturn is a finite-size effect caused by periodic boundary conditions.

A comparison of our QMC results with those from BCS and DMRG calculations are shown in Fig. 2(a). Clearly, the predictions from the two quite different numerical methods agree, provided we average the DMRG results as discussed above. For purposes of comparison, we also show the prediction of the BCS approximation. It is qualitatively different from what is required from the exact solution. Figure 2(b) shows the difference in the DMRG results when computed
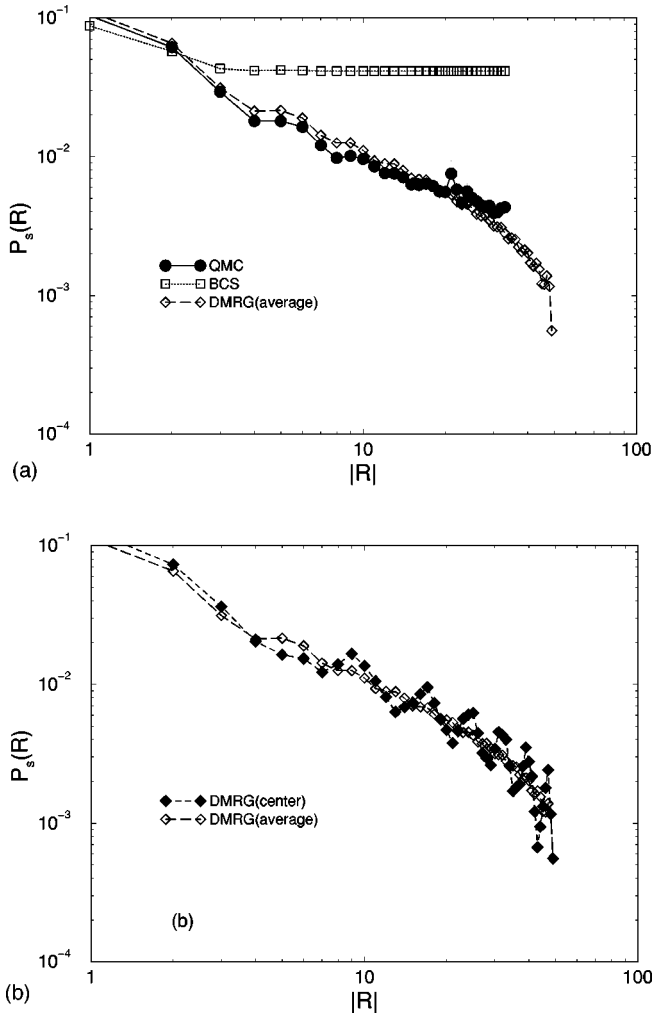
(a)

(b)

FIG. 2. The on-site s-wave pairing correlation function $P_s(R)$ as a function of the distance $|R|$ between pairs for a $U/t=2$ chain of length $L=50$. (a) Comparison of the results of the BCS approximation with a QMC calculation that used Eq. (19) and a DMRG calculation that used Eq. (21). (b) Comparison of the DMRG results for the two different ways, Eqs. (20) and (21), of estimating the correlation function.

for the two different ways of averaging, that is, when computed from Eqs. (20) and (21).

In short, both the DMRG and QMC predictions agree well with each other and with the exact prediction of the Bethe ansatz solution for the asymptotic form of the pairing correlation function at large distances. As expected, the BCS approximation is qualitatively incorrect for this same function.

B. Squares

In two dimensions, an exact analytic solution for the Hubbard model does not exist. Within statistical error, the QMC approach, however, provides an exact numerical solution. In this subsection we are principally concerned with comparing predictions of the BCS approximation with those of the exact QMC simulations.

In Fig. 3, we show the QMC and BCS $P_s(R)$ as a function of the distance R for an 8×8 lattice with $U/t=1$, 2, and 4. The curves show the same behavior: The correlations rapidly drop in magnitude over a distance of a few lattice spac-
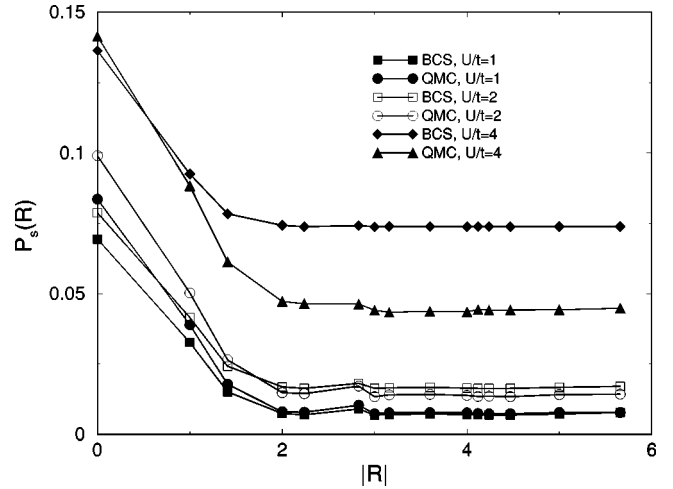

FIG. 3. The QMC and BCS on-site s-wave pairing correlation function $P_s(R)$ as a function of the distance $|R|$ between pairs for a 8×8 lattice and $U/t=1$, $U/t=2$, and $U/t=4$.

ings and then stay constant over the remainder of the distances. The constant behavior at these larger distances is a signature of ODLRO, if the distances extended to infinity. As the results go from $U/t=1$ to $U/t=4$, the agreement between the QMC simulations and the BCS approximation for lattices of the same size progressively worsens. Beyond $U/t=1$, the quantitative agreement is poor. One also sees that as U/t increases, the magnitude of the pairing correlations increases. At large distances, if there is ODLRO, the pairing correlation function becomes asymptotically equal to $\langle \Delta_s \rangle^2$. In the BCS approximation, U times $\langle \Delta_s \rangle$ equals the energy gap, and this gap becomes exponentially small when decreasing U/t to 0 and proportional to U/t when increasing U/t to infinity. However, as noted before, the attractive Hubbard model is gapless if it has on-site s-wave ODLRO.[15]

While we computed several cases for $U/t=8$, the statistical error was considerably larger and hence we do not show these results. However, in all cases computed, as we increased the magnitude of U/t, we never saw the QMC and BCS results approach each other. In fact, as we increased U/t beyond 1, their difference continuously increased. In Fig. 4, we show both the on-site and extended s-wave pairing correlation functions as a function of distance for $U/t=4$ and a 14×14 lattice. In the inset we eliminated the short distance part to emphasize the flat large distance behavior for both correlation functions. By averaging over this flat behavior we estimated both $\langle \Delta_{s*} \rangle^2$ and $\langle \Delta_s \rangle^2$ and attempted to verify that the ratio is proportional to $(-U-2\mu)^2/t^2$ as stated by Eq. (5). Because most of our simulations were done for fixed particle numbers and closed-shell fillings, the estimation of μ was difficult. Using a variation of the present method[18] that allows an estimation of μ, we found $\mu=-2.77$ for a 8×8 system with $U/t=4$. Using this same value of μ for the 14×14 system with $U/t=4$ yields $(-U-2\mu)^2/t^2=2.37$ which compares very well to the value of 2.40(3) estimated from the figures. We also observed that the ratio of the expectation values for the on-site and extended s-wave order parameters was *exactly* obeyed in the BCS approximation, provided the BCS value of μ was used. In Appendix A we present the analysis leading to this result. We also observed that the long-range values of both the on-site
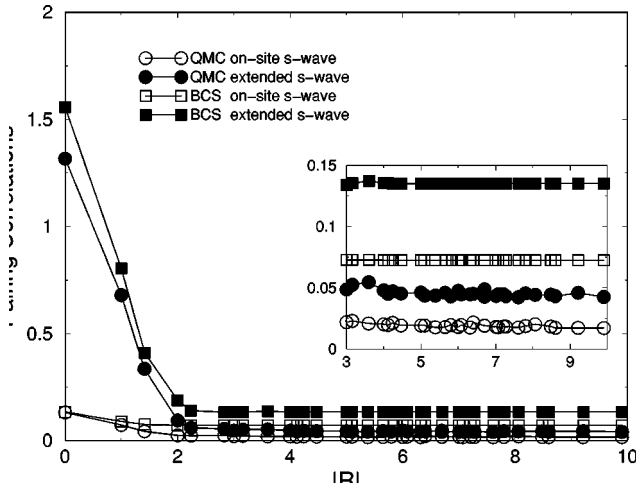
FIG. 4. The QMC and BCS on-site and extended s-wave pairing correlation functions $P_s(R)$ as a function of the distance $|R|$ between pairs for $U/t=2$ and a 14×14 lattice. The inset shows the large distance behavior of these same functions.

and extended s-wave pairing correlation functions do not vary monotonically with lattice size. We illustrate this in Fig. 5 by plotting both the QMC and BCS results for $\langle\Delta_s\rangle$ as a function of the reciprocal of the number N of lattice sites for both $U/t=2$ and $U/t=4$. Within the BCS approximation one can compute $\langle\Delta_s\rangle$ directly for any lattice size.

In Fig. 5(a), the BCS result for $U/t=2$ clearly does not converge to the thermodynamic limit monotonically. The
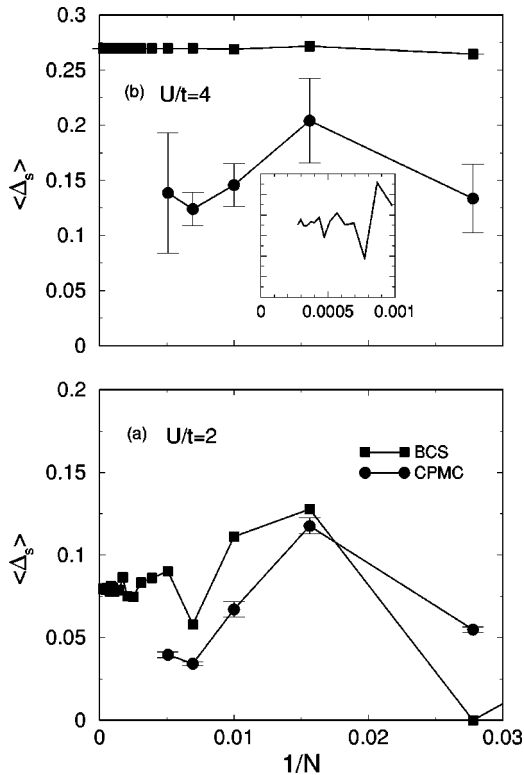
FIG. 5. The expectation value of the on-site s-wave order parameter $\langle\Delta_s\rangle$ as a function of the reciprocal of the size N of a square lattice. In both (a) and (b) the QMC results are compared to those of the BCS approximation. In (a), $U/t=2$. In (b), $U/t=4$ and the inset shows the behavior of the BCS predictions for small values of the reciprocal of the lattice size.

same lack of monotonicity is apparent in the variation of the QMC results. Because the BCS and QMC results are quantitatively different, we see no reason why the QMC results might extrapolate to the BCS result, but more importantly, we do not see how to extract an accurate value of $\langle\Delta_s\rangle$ in the thermodynamic limit, although it is clear from our results that it is a finite value and therefore there will be ODLRO in the thermodynamic limit. In Fig. 5(b), we show similar curves for $U/t=4$. The apparent monotonicity of the BCS result is deceptive, as illustrated in the inset to this figure. The more important point is that the BCS results approach the thermodynamic limit for $U/t=4$ case more rapidly than they did for the $U/t=2$ case. This trend is very general and suggests that the QMC results for larger values of U/t will also converge more rapidly to the thermodynamic limit. Large interactions reduce fermion shell effects. Unfortunately both the necessarily large values of U/t and lattice sizes appear inaccessible with our simulation method. For $U/t=1$ we estimate that the BCS approximation has approached the thermodynamic limit within a percent for lattices of the order of 60×60; for $U/t=8$ our estimate is for lattices of the order of 10×10. As mentioned before, at $U/t=8$ the QMC results have large statistical errors in the back-propagation estimate of the pairing correlation functions.

In summary, for on-site s-wave pairing correlations, we find that the QMC and BCS results agree in the weak-coupling limit. While the QMC results show a necessary signature of ODLRO, we were unable to extrapolate accurately our results for the order parameter to the thermodynamic limit.

C. Ladders

An alternate way to reach the two-dimensional thermodynamic limit is extrapolating from a ladder structure of fixed, but long, length L by letting the number of legs M become large. Here we report our results from the use of this strategy.

We built up the ladder structures by coupling 1, 2, and 3 additional chains to the one-dimensional chain and making the interchain and intrachain hopping amplitudes equal. We used periodic boundary conditions in the x (long) direction and open boundary conditions in the y (short) direction. We call this a cylindrical boundary condition. For the on-site s-wave pairing correlation function we computed it only along the x direction, using

$$P_s(R)=\frac{1}{L}\sum_{i_0}\langle\Delta_s^\dagger(i_0+R)\Delta_s(i_0)\rangle, \qquad (22)$$

where the i_0 are lattice sites along one of the central legs of the ladder. For a three-legged ladder, the sites in the x direction are on the central leg. For a two-legged ladder, we used just one of the legs. By symmetry, the chain-directed pairing correlations are the same on each leg. For a four-legged ladder, we just used one of the two central legs.

To provide some perspective, we first present in Fig. 6 plots of the energy as a function of system size. In particular, in Fig. 6(a) is the energy per site for a $U/t=2$ chain as a function of the reciprocal of chain length. The variation with length is smooth and monotonic. Linearly extrapolating this
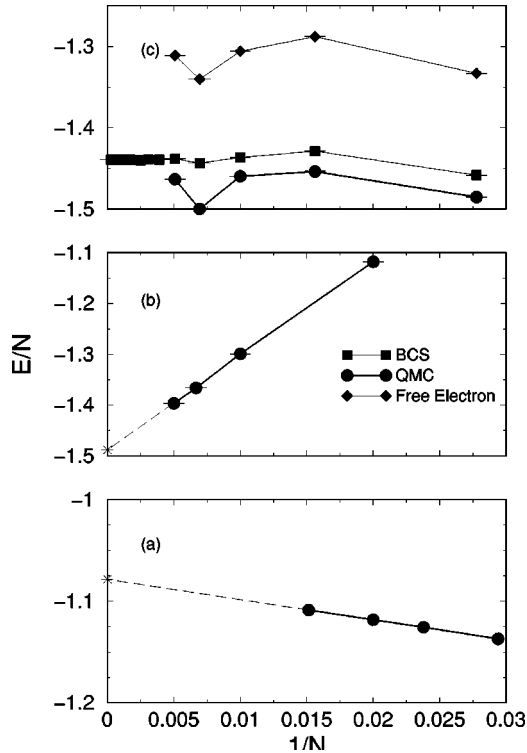
FIG. 7. The QMC on-site s-wave pairing correlation function $P_s(R)$ as a function of the distance $|R|$ between pairs for $U/t=2$, and two and three-legged ladders of different lengths.

FIG. 6. The QMC energy per site E/N as a function of the reciprocal of the number N of lattice sites for $U/t=2$ systems. (a) Chains ($N=L$), (b) ladders ($N=L\times M$), and (c) squares ($N=L\times L$). For squares the free-electron and BCS results are also shown. For chains and ladders, the QMC curves smoothly and linearly extrapolate to the thermodynamic limit indicated by the starburst symbols at $1/N=0$.

data to infinite length, we find an energy per site of $-1.079(1)$ which is within statistical error of the Bethe ansatz value of -1.079.[25] In Fig. 6(b) is the energy per site as a function of the reciprocal of the number of legs M for a ladder of length $L=50$. The variation is smooth and monotonic and extrapolates to a value of $-1.49(1)$, a value similar to the one we found from the QMC simulations for the two-dimensional lattice. This is not surprising since, although the extrapolating function can be shape dependent, the energy is a bulk quantity, i.e., independent of the way one performs the thermodynamic limit. These two-dimensional QMC results are shown in Fig. 6(c) for the non-interacting case and for the interacting case computed by both the BCS approximation and the QMC method. The variation is neither smooth or monotonic. Additionally it tracks the noninteracting problem. This tracking supports a claim that the nonmonotonic variations are caused by shell effects that are obvious and inherent to non-interacting fermion problems. For the s-wave pairing correlation function, a typical result is shown in Fig. 7. Similar to the one-dimensional case (Fig. 1), the curves for increasing ladder length lie on top of those for shorter lengths. In contrast to the one-dimensional case, however, distinct oscillations exist but the overall trend is a decrease in magnitude with increasing distance. For the two- and three- legged cases we fitted the top and bottom envelopes of the oscillations to the power-law decay (17) and found the two decays rates to be close but not the same. These exponents were also close to
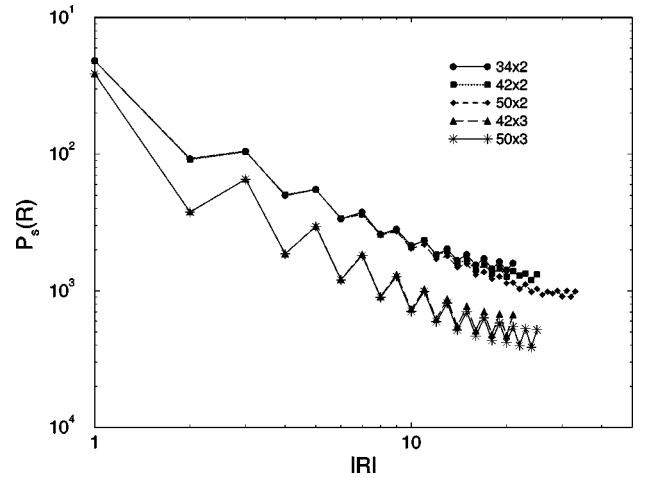
the one-dimensional value (Table I). An important observation is the overall magnitude of the pairing correlations at first decreasing below the one-dimensional value and then, as we built up the ladder structure to four legs, increasing above the three-leg value. For a ladder of length $L=50$, the variation of the s-wave pairing correlation function with the number of legs is shown in Fig. 8. A typical fit to determine the exponents of decay is shown in the inset. Other fitted values are given in Table I. We note that while the exponent does not change much from the one-dimensional case to the two and three-legged ladder cases, it does decrease significantly when the fourth leg is added.

We remark that using the BCS approximation, we computed the pairing correlations for the same system sizes but with periodic boundary conditions in both directions. While this approximation always showed ODLRO, its order parameter $\langle \Delta_s \rangle$ showed the same trend as we obtained from the QMC simulations: In going from one to three-legs, the value
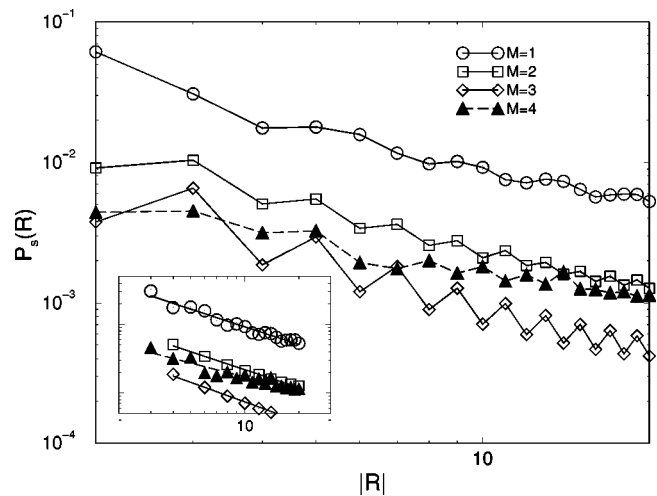

FIG. 8. The QMC on-site s-wave pairing correlation function $P_s(R)$ as a function of the distance $|R|$ between pairs for a $U/t=2$ ladder of length 50 as a function of the number of legs M. The inset shows the long-range behavior of these correlations fitted to the inverse power-law function (17).

of the order parameter at first monotonically decreased but then increased relative to the value of the three-legged ladder when the fourth leg was added.

D. Dimensional crossover

What type of variation with ladder width should one expect? Recently finite temperature QMC studies of quantum spin-$\frac{1}{2}$ ladders found nonmonotonic variations with the number of legs.[26–28] More specifically, the dynamic susceptibilities of even-legged ladders had spin gaps while those of odd-legged ones did not. The size of the spin gap rapidly decreased with increasing number of legs and is a result of topological considerations similar to those associated with Haldane gaps in one-dimensional chains. For fixed, but large, ladder lengths the uniform susceptibility vanished as the temperature was lowered and then the number of legs extrapolated to infinity. This susceptibility however extrapolated to a nonzero value if at low temperatures the two-dimensional results were extrapolated to the thermodynamic limit. Proper extrapolation of this system to the thermodynamic limit appears to be an unsolved problem. The theoretical and experimental situation has received several recent reviews.[29,30]

Turning from quantum critical phenomena to the finite temperature critical behavior and using the two-dimensional Ising model as an example, we can easily study the dimensional crossover from one to two dimensions and the extrapolation of two-dimensional results to the thermodynamic limit. We, in fact, were able to derive exact results, given in Appendix B, for the spin-spin correlations for such finite systems. Using these exact results we computed the spin-spin correlation function as a function of distance along the central leg for several illustrative cases. For the calculations presented in Fig. 9, we fixed the reciprocal of the critical temperature at its bulk value of $\frac{1}{2}\ln(\sqrt{2}+1)\approx 0.44$, chose a long ladder length of 200 lattice sites, and computed the correlation function for various number of legs. What is seen is a smooth but gradual transition from the expected exponential decay in one dimension to the expected power-law decay in two dimensions. Proper extrapolation of this system to the thermodynamic limit is an exactly solvable problem.[31]

What is the relevance of the studies on these spins systems to our QMC simulations? From studies in finite-temperature critical phenomena, one suggestion on the controlling physics of a dimensional crossover is the type of behavior depending on the relative size of the dominant correlation length to the width of the system.[32] This insight was developed in part from analytic studies of D-dimensional ladders sized $\infty \times \infty \times \cdots \times \infty \times M$ and scaling its behavior to a $(D+1)$-dimensional system by letting $M \to \infty$. In going from one to two dimensions, as long as one is on the critical surface, one expects the long-range behavior to be one-dimensional-like if the correlation length is larger than the width and two-dimensional-like if it is smaller. The various correlation functions we computed for the Hubbard model, such as charge-charge, spin-spin, and pair-pair, rapidly decayed over a distance of several lattice spacings from their on-site value, suggesting our system sizes were large enough so that if we were on the quantum critical surface, our phys-
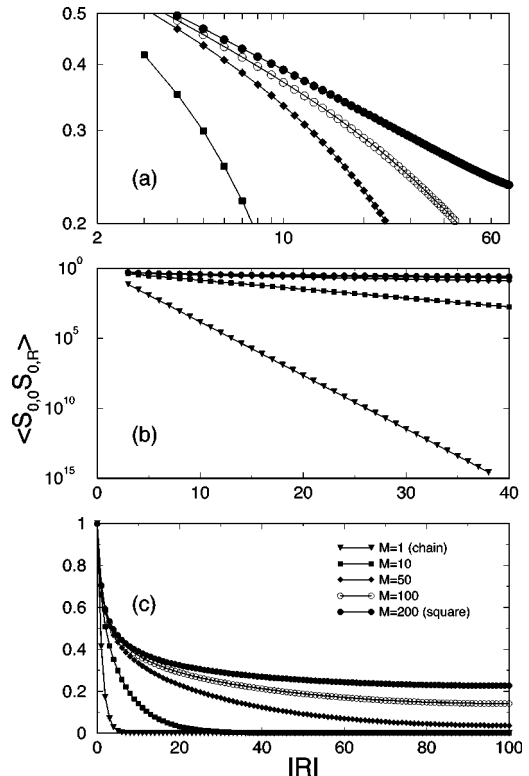

FIG. 9. The spin-spin correlation function for an Ising ladder of length $L=200$ as a function of the distance $|R|$ between spins and of the number of legs M. The temperature is at the bulk critical value, and the distance $|R|$ is along a central leg in the x direction. Cylindrical boundary conditions were used.

ics would be more two-dimensional-like than one-dimensional-like. We find that it appears to be the other way around.

The picture so appropriate for finite-temperature critical phenomena established for classical systems might not be appropriate to our fermion simulations because the system sizes are too small and are dominated by shell effects, a phenomenon intrinsic to quantum fermion systems. In Fig. 10, we plot the band structure of the free-electron case for one, two, three, and four legged ladders of infinite length with cylindrical boundary conditions. The horizontal line represents the Fermi energy for an electron density of 1/2. For one leg, the one-dimensional case, there is one band. For two-legs there are two bands but only the lower band is filled. While the entire system is quarter filled, the one-
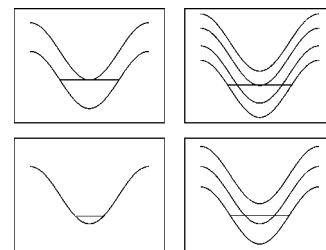

FIG. 10. Bandstructure of the noninteracting problem on one-, two-, three-, and four-legged ladders. Cylindrical boundary conditions are applied. The long length L is infinite, and the horizontal line represents the Fermi energy for a quarter filled system.
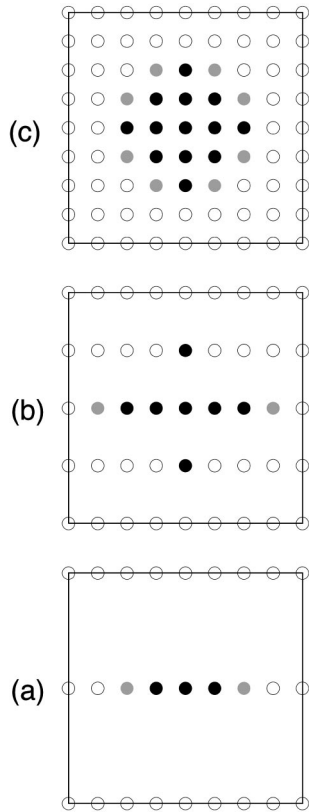
FIG. 11. The allowed **k** states for a 2×8, 4×8, and 8×8 noninteracting problem with periodic boundary conditions. Illustrated are which **k** states are occupied for quarter filling of an equal number of up- and down-spin electrons. A black dot denotes double occupancy, an open circle represents no occupancy, and a grey dot represents the degenerate state comprising the open shell.

dimensional-like lower band is half filled. Not surprisingly then is the one-dimensional-like decay rate of the pairing correlations. For three and four legs there are three and four bands. More than one band is participating but the situation is not yet two-dimensional-like. This simple band picture therefore provides some qualitative basis for understanding our data. This understanding suggests, at least for the sizes of the systems we were able to study, that the length scale interpretation of dimensional crossover is not yet applicable.

As still another way of looking at the finite-size effects we present Fig. 11 which displays the allowable **k** values for noninteracting 2×8, 4×8, and 8×8 lattices with periodic boundary conditions. For quarter filling the black dots are occupied by an up- and down-spin electron, the gray dots are the degenerate states in the open shell, and the open dots are unoccupied. Clearly for 2×8 the occupied **k** states are those of a one-dimensional lattice. This situation changes little in the 4×8 case, but has significantly changed for the 8×8 case. Obviously in the noninteracting case the dimensional crossover requires more than just a few legs.

While finite-size shell effects may explain the nonmonotonic variations we observed, we emphasize that the nature of the variation of the pairing correlation to crossover from one to two dimensions was not revealed in our simulations. We note than even in the apparently simpler classical Ising model the crossover was slow.

V. CONCLUDING REMARKS

We presented an extensive QMC study of pairing correlations in the attractive Hubbard model on chains, ladders, and squares. While still computationally intensive, the QMC method we used is free of the fermion sign problem that would prevent a similar study for the repulsive Hubbard model. By using a method free of the sign problem, we obtained results that apart from statistical errors are exact. In several instances we re-enforced this exactness by reproducing behavior predicted by exact analysis. For example, for chains we got the correct asymptotic behavior of the on-site s-wave pairing correlation function. For squares, we verified Zhang's relation between the on-site and extended s-wave order parameters. Several of our ambitious computational objectives were, however, limited by the size of the systems and interactions strengths we could afford to simulate. Still, we demonstrated the validity of the BCS approximation in the weak-coupling limit for a short-ranged interaction and highlighted several important unresolved issues about finite-scaling of fermion systems.

To a degree, the finite-size and shell effects exhibited by our results are expected. Such effects have been reported before.[17,33,34] The difficulty we had in trying to extrapolate beyond them to the thermodynamic limit was unexpected. Part of the surprise follows from QMC simulations of the attractive Hubbard model always having an easier time revealing a signature of ODLRO than simulations of the repulsive model. Years ago, in fact, ODLRO was reported for the attractive model via a QMC simulation.[7] How we attempted to establish ODLRO in this paper, however, differs from how it was attempted in that previous work. There, the uniform susceptibility

$$\chi_s = \frac{1}{N} \sum_R P_s(R) \qquad (23)$$

was extrapolated to the thermodynamic limit. While this is an appropriate quantity for very large system sizes, it is now appreciated that for small systems, it is often dominated by the values of $P_s(R)$ near $R = 0$. These values merely measure local spin and charge fluctuations. Directly examining the long-distance behavior of $P_s(R)$, as done here, is a more appropriate procedure.

Re-examining Fig. 3 of Ref. 7, we notice the following: The values of χ_s for small lattices were excluded from the extrapolation. The values for the larger lattice sizes fluctuated about the fit by amounts larger than the statistical error. We do not doubt that a proper extrapolation will yield a non-negative value for χ_s. Noting that χ_s is roughly $\langle \Delta_s \rangle^2$, we remark that their numerical values for $\langle \Delta_s \rangle$ are consistent with ours.

From Fig. 3 of Ref. 7, we also notice how smoothly the uniform susceptibility for the charge-density wave extrapolated to the thermodynamic limit. In the present work, we recall the smooth and linear variation of the energy of the chains and the ladders with size in contrast to the erratic variation for the squares. The finite-size effects influence different quantities and systems differently. While one expects these effects, where they appear appreciably is a bit less predictable.

What is curious is the control the shell structure of the noninteracting problem has on the behavior of the interacting system. If one were to examine the variation of energy of the two-dimensional Hubbard model as a function of electron density, one would see shell locations defined by the noninteracting problem and the energy in a shell to a very good approximation varying nearly linearly with electron density.[33,17,34] The interactions do change the slope (chemical potential) of this variation from the noninteraction value; however, this nearly linear variation suggests the presence of different sets of nearly degenerate ground states as the electron density varies form shell to shell. One expects the interaction to destroy the degeneracy in the shell of the noninteracting problem so that shell effects in the interacting problem would be less than those in the noninteracting problem. This expectation is not fully supported by the data for all properties of the system.

One of our objectives was establishing how large must the system be before we can say it is in a superconducting state. Over 40 years ago, Anderson[35] asked how small can superconducting metal particles be before they lose their superconducting properties. He asserted the cutoff came when the gap near the Fermi surface induced by the small size becomes larger than the superconducting gap. There is evidence for the validity of this condition from experimental studies of the superconducting properties of metal clusters. What happens if the superconductor, as is the case for the attractive Hubbard model, is gapless? On the other hand, is the finite attractive model approximately a gapped superconductor? If so, are our results suggesting the gaps are small?

What are the implications of our results for establishing ODLRO in the repulsive Hubbard model? The behavior of the repulsive model is quite different than the behavior of the attractive model. For any size of the repulsive model studied so far, the difficulty is finding pairing correlations larger than those of the noninteracting problem.[36] In the thermodynamic limit the noninteracting problem is not superconducting so whatever long-range correlations seen for small systems must suppressed in larger systems. In the repulsive model, d-wave pairing correlations are stronger than the s-wave pairing correlations, and as the system size was increased, the magnitude of the d-wave pairing correlations systematically vanished.[36,18] What our results underscore is the care needed to establish that any observed enhancement of the d-wave pairing correlations is an intrinsic effect and not a finite-size effect.

We comment that all results reported here are for a single electron filling. All the properties studied are a function of filling so at some other fillings, it might be easier to extrapolate to the thermodynamic limit and it might be possible that the BCS approximation remains in quantitative agreement with the QMC simulations for larger values of U/t. In fact, a few simulations for $\langle n \rangle = 0.875$ for 4×4, 6×6, and 8×8 lattices showed only a weak variation in the results for the pairing correlation function.

While we simulated systems at other fillings, these simulations were neither extensive or systematic enough to establish conclusions other than those now being reported. Also in building up the ladder to a square, we took quite long ladders which restricted the number of legs we could afford to simulate. We made the ladder long so the pairing properties of the
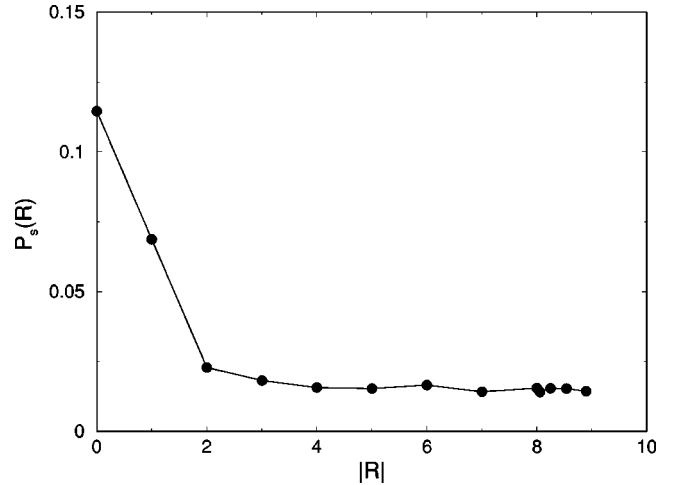

FIG. 12. The QMC on-site s-wave pairing correlation function $P_s(R)$ as a function of the distance $|R|$ between pairs for a rectangular quarter filled $U/t = 2$ lattice of size 16×8.

chain clearly matched the predications of the Bethe ansatz solution of the infinite chain. It might be possible to see the dimensional crossover and extrapolate to the bulk two-dimensional properties from shorter but wider ladders. For example, in Fig. 12 we show $P_s(R)$ for a 16×8 ladder at $U/t = 2$. The flatness suggests possible ODLRO consistent with the results for the square geometry.

What are possible ways of handling the finite-size effects? One way, suggested by Bormann, Schneider, and Frick,[37] is adjusting U/t for different system sizes so the BCS approximation for $P_s(R)$ closely approximates the one from the QMC simulations, subtracting this approximation from the QMC results, and then extrapolating the differences to the thermodynamic limit. After this, then one would add to this result the BCS results for an infinite system. (Actually, Bormann, Schneider, and Frick did this for χ_s.) We did not try this procedure because it is related to another one, scaling the vertex correction. Here, one replaces averages like $\langle c^\dagger c^\dagger c c \rangle$ with $\langle c^\dagger c^\dagger c c \rangle - \langle c^\dagger c \rangle \langle c^\dagger c \rangle$ and studies the size dependence of the remainder which is called the vertex contribution.[38] In spot checks, we found no significantly different scaling behavior between the vertex and full contributions.

Another way to remove finite-size effects is the phase averaging method suggested for exact diagonalization studies by Loh and co-workers[39] and recently adopted for QMC simulations by Ceperley.[40] In this procedure, one replaces the hopping amplitude t at the boundary by $te^{i\phi}$ and obtains various physical quantities as a function of ϕ. Then one averages these quantities over ϕ. Loh and co-workers give a justification and demonstration of the method. In exact diagonalization studies, one just does a sequence of diagonalizations for different values of ϕ. In a Monte Carlo method for computational efficiency it is necessary to treat ϕ as another stochastic parameter and then let the random walk do the averaging. To do this one needs to change the QMC method. In the applications contemplated by Ceperley, this means changing from the fixed-node to the fixed-phase method.[41] In our case we are developing an analog of the fixed-phase method, called the constrained phase.[42] Hopefully we will be able to report results from this method soon.

Finally, we would like to emphasize that this paper has

been dealing exclusively with systems having a homogeneous long-range phase coherence. There is a rapidly growing body of experimental evidence suggesting that inhomogeneously textured (intrinsically nanoscale) phases characterize the quantum state of high-temperature superconductors. It is possible that the superfluid density characterizing that state is inhomogeneous. We believe that an extension of the attractive Hubbard model including inhomogeneous terms (mimicking stripes) could be the starting point to understand the fundamental problem of inhomogeneous superfluids.

APPENDIX A: BCS EQUATIONS

In this appendix we present the key equations used in our BCS calculations. Some are well documented while others are not. For completeness and convenience we give them here.

First to establish notation, we take Eq. (3) as the Hamiltonian for a lattice of N sites and rewrite it in $\mathbf{k}$ space:

$$H = \sum_{\mathbf{k},\sigma} \epsilon_{\mathbf{k}} n_{\mathbf{k},\sigma} - \frac{U}{2N} \sum_{\substack{\mathbf{k},\mathbf{k}',\mathbf{q} \\ \sigma=\uparrow,\downarrow}} c^\dagger_{\mathbf{k},\sigma} c^\dagger_{\mathbf{k}',-\sigma} c_{\mathbf{k}'+\mathbf{q},-\sigma} c_{\mathbf{k}-\mathbf{q},\sigma},$$

(A1)

using $\epsilon_{\mathbf{k}} = -2t(\cos k_x + \cos k_y)$ and assuming periodic boundary conditions in all spatial directions. We used the BCS wave function (2) with $\mathbf{k}$-independent relative phase φ:

$$|BCS(\varphi)\rangle = \prod_{\mathbf{k}} (u_{\mathbf{k}} + v_{\mathbf{k}} e^{i\varphi} c^\dagger_{\mathbf{k},\uparrow} c^\dagger_{-\mathbf{k},\downarrow}) |0\rangle.$$

(A2)

The effective mean-field Hamiltonian, resulting from the neglect of pairing fluctuations, is

$$H_{BCS} = \sum_{\mathbf{k},\sigma} \xi_{\mathbf{k}} n_{\mathbf{k},\sigma} - \Delta \sum_{\mathbf{k}} (c^\dagger_{\mathbf{k},\uparrow} c^\dagger_{-\mathbf{k},\downarrow} + c_{-\mathbf{k},\downarrow} c_{\mathbf{k},\uparrow}) + \frac{UN_e^2}{4N},$$

(A3)

where $N_e = \langle \hat{N}_e \rangle = 2\sum_{\mathbf{k}} v_{\mathbf{k}}^2$ is the average number of electrons and $\Delta = (U/N)\sum_{\mathbf{k}}\langle c^\dagger_{\mathbf{k},\uparrow} c^\dagger_{-\mathbf{k},\downarrow}\rangle = (U/N)\sum_{\mathbf{k}} u_{\mathbf{k}} v_{\mathbf{k}}$ is the BCS gap, and $\xi_{\mathbf{k}} = \epsilon_{\mathbf{k}} - \mu - UN_e/2N$. The value of the energy was calculated from

$$\langle H_{BCS} \rangle = \langle H - \mu \hat{N}_e \rangle$$
$$= 2\sum_{\mathbf{k}} (\epsilon_{\mathbf{k}} - \mu) v_{\mathbf{k}}^2 - \frac{U}{N}\left[\left(\frac{N_e}{2}\right)^2 + \left(\frac{N\Delta}{U}\right)^2 \right]$$

(A4)

and μ and Δ were determined by self-consistently solving

$$\sum_{\mathbf{k}} \left[1 - \frac{\xi_{\mathbf{k}}}{E_{\mathbf{k}}} \right] = N_e,$$

(A5)

$$\frac{U}{2N} \sum_{\mathbf{k}} E_{\mathbf{k}}^{-1} = 1,$$

(A6)

where $E_{\mathbf{k}} = \sqrt{\xi_{\mathbf{k}}^2 + \Delta^2}$. With these values of μ and Δ we determined $u_{\mathbf{k}}, v_{\mathbf{k}}$ from

$$2u_{\mathbf{k}} v_{\mathbf{k}} = \frac{\Delta}{E_{\mathbf{k}}},$$

(A7)

$$u_{\mathbf{k}}^2 - v_{\mathbf{k}}^2 = \frac{\xi_{\mathbf{k}}}{E_{\mathbf{k}}}.$$

(A8)

A quantity central to this work is the s-wave superconducting pairing correlation function $P_s(\mathbf{R}) = \langle \Delta_s^\dagger(\mathbf{R}) \Delta_s(0) \rangle$. Within the BCS approximation it is

$$P_s(\mathbf{R}) = \left(\frac{\Delta}{U}\right)^2 + \frac{N_e}{2N} \delta_{\mathbf{R},0} - F(\mathbf{R}),$$

(A9)

where the function $F(\mathbf{R})$

$$F(\mathbf{R}) = \frac{1}{N^2} \sum_{\mathbf{k},\mathbf{k}'} e^{i(\mathbf{k}'-\mathbf{k})\cdot\mathbf{R}} u_{\mathbf{k}'}^2 v_{\mathbf{k}}^2$$

(A10)

vanishes in the limit $|\mathbf{R}| \to \infty$.

To establish the proportionality between the s-wave and extended s-wave order parameters, we considered the Heisenberg equation of motion for $\Delta_s(i) = c_{i,\downarrow} c_{i,\uparrow}$:

$$-i \frac{\partial \Delta_s(i)}{\partial t} = [H_{BCS}, \Delta_s(i)].$$

(A11)

It is straightforward to show that

$$[H_{BCS}, \Delta_s(i)] = (UN_e/N + 2\mu)\Delta_s(i) + t\Delta_{s*}(i)$$
$$- \Delta(n_{i,\uparrow} + n_{i,\downarrow} - 1).$$

(A12)

Then using $\langle [H_{BCS}, \Delta_s(i)] \rangle = 0$ for an equilibrium state, we find

$$\langle \Delta_{s*}(i) \rangle = \frac{-U - 2\mu}{t} \langle \Delta_s(i) \rangle = \frac{-U - 2\mu}{t} \left(\frac{\Delta}{U}\right),$$

(A13)

where the extended s-wave pair field operator is defined by

$$\Delta_{s*}(i) = \sum_{\delta = \pm \hat{x}, \pm \hat{y}} (c_{i,\downarrow} c_{i+\delta,\uparrow} - c_{i,\uparrow} c_{i+\delta,\downarrow}).$$

(A14)

This fundamental relation is formally the same as the one found by Zhang[16] for the exact solution of the Hubbard model. We note, however, that the chemical potential and expectation values in Eq. (A13) are BCS ones.

In the strong-coupling regime ($U/t \to \infty$), the chemical potential $\mu = -U/2$ and the gap $\Delta = \frac{1}{2} U \sqrt{1 - (N_e/N - 1)^2}$, therefore

$$\left(\frac{\Delta}{U}\right)^2 \to \frac{1}{4}\left[1 - \left(\frac{N_e}{N} - 1\right)^2 \right]$$

(A15)

and in that limit $\langle\Delta_{s*}\rangle=0$ and

$$|\text{BCS}(0)\rangle=\prod_i\left[\sqrt{1-\frac{N_e}{2N}}+\sqrt{\frac{N_e}{2N}}c_{i\uparrow}^\dagger c_{i\downarrow}^\dagger\right]|0\rangle. \tag{A16}$$

While not used in any of the results reported here, another relation we derived and found useful in other contexts is a simple way to project from the BCS wave function the component corresponding to a fixed number of particles. Although in the thermodynamic limit one can ignore exact particle number conservation, for a finite system, one often cannot because the particle number fluctuations $\langle\hat{N}_e^2\rangle-\langle\hat{N}_e\rangle^2=4\Sigma_\mathbf{k}u_\mathbf{k}^2v_\mathbf{k}^2$, inherent in the BCS wave function, can be large. To project out the N_e-particle component, one uses

$$|\Psi_{N_e}\rangle=\frac{1}{2\pi}\int_0^{2\pi}d\varphi e^{-i\varphi N_e/2}|\text{BCS}(\varphi)\rangle. \tag{A17}$$

By directly doing the implied integration over the phase, one can show that the amplitude $\langle\text{BCS}(0)|\Psi_{N_e}\rangle=\langle\Psi_{N_e}|\Psi_{N_e}\rangle=\omega_{N_e}$ where $\Sigma_{N_e}\omega_{N_e}=1$. To find ω_{N_e} one can use the recursion relation

$$N_p\omega_{N_p}=\omega_{N_p-1}\sum_\mathbf{k}\left(\frac{v_\mathbf{k}}{u_\mathbf{k}}\right)^2$$
$$+\sum_{j=1}^{N_p-1}(-1)^j\omega_{N_p-(j+1)}\sum_\mathbf{k}\left(\frac{v_\mathbf{k}}{u_\mathbf{k}}\right)^{2(j+1)}, \tag{A18}$$

where $N_p=N_e/2$ is the number of pairs. We also note that $|\text{BCS}(0)\rangle=\Sigma_{N_e}|\Psi_{N_e}\rangle$.

APPENDIX B: ISING LADDERS

In this appendix we state the main equations necessary to study the crossover from one to two dimensions in a system of classical Ising spins. We present analytical expressions from which various observables are derivable. In particular, we state those equations necessary to study the large-distance behavior of the spin-spin correlation function near and at the two-dimensional critical point.

Because of the extensive literature on the Ising model, we will present only the results relevant for a $L\times M$ lattice, which have not been explicitly documented to our knowledge. As close as we could, we followed the notation and methodology in Ref. 31.

The M-ladder Ising Hamiltonian in the absence of an external magnetic field is

$$H=-J_1\sum_{i=-M_-}^{M_+}\sum_{j=1-\bar{N}}^{\bar{N}}S_{i,j}S_{i,j+1}$$
$$-J_2\sum_{i=-M_-}^{M_+-1}\sum_{j=1-\bar{N}}^{\bar{N}}S_{i,j}S_{i+1,j}, \tag{B1}$$

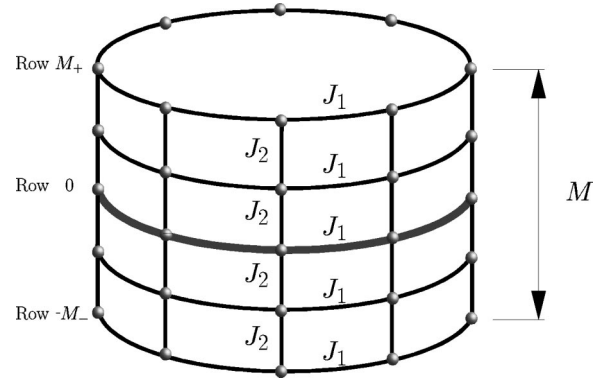where cylindrical boundary conditions $(S_{i,1-\bar{N}}=S_{i,1+\bar{N}})$ are used, $S_{i,j}=\pm1$, and

FIG. 13. The cylindrical geometry used for the Ising model ladder with M legs.

$$M_++M_-+1=M \quad\text{(number of rows)}$$
$$2\bar{N}=L \quad\text{(number of columns)} \tag{B2}$$

Figure 13 presents a schematic representation of the model Hamiltonian H. The partition function $\mathcal{Z}_{ML}$ is

$$\mathcal{Z}_{ML}=[2\cosh(\beta J_1)]^{ML}(\cosh(\beta J_2))^{(M-1)L}\text{Pf}[\mathcal{A}], \tag{B3}$$

where the Pfaffian of the antisymmetric matrix $\mathcal{A}$ is

$$\text{Pf}^2[\mathcal{A}]=\det\mathcal{A}=\prod_\theta\{|1+z_1e^{i\theta}|^{2M}\lambda^M[v^2+\alpha^{-2M}\bar{v}^2]\}, \tag{B4}$$

with $\theta=\pi(2n-1)/L(n=1,2,\ldots,L),z_{1(2)}=\tanh(\beta J_{1(2)}),$

$$\lambda=\frac{z_2(1-z_1^2)\alpha}{|1+z_1e^{i\theta}|^2}, \quad\bar{\lambda}=\frac{z_2(1-z_1^2)}{|1+z_1e^{i\theta}|^2\alpha} \tag{B5}$$

$$\alpha=\frac{1}{2z_2(1-z_1^2)}\left\{(1+z_1^2)(1+z_2^2)\right.$$
$$-z_1(1-z_2^2)[e^{i\theta}+e^{-i\theta}](1-z_2^2)$$
$$\left.\times\sqrt{(1-\alpha_1e^{i\theta})(1-\alpha_1e^{-i\theta})\left(1-\frac{e^{i\theta}}{\alpha_2}\right)\left(1-\frac{e^{-i\theta}}{\alpha_2}\right)}\right\}, \tag{B6}$$

$$\alpha_1=\frac{z_1(1-|z_2|)}{1+|z_2|}, \quad\alpha_2=\frac{z_1^{-1}(1-|z_2|)}{1+|z_2|}, \tag{B7}$$

$$v^2=\frac{1}{2}\left(1+\frac{z_2^2-[4z_1^2\sin^2(\theta)+(1-z_1^2)^2]/|1+z_1e^{i\theta}|^4}{\bar{\lambda}-\lambda}\right), \tag{B8}$$

$$\bar{v}^2=1-v^2.$$

We were mainly interested in studying the spin-spin correlation function along the central row (as indicated in Fig. 13). This function is given by

$$\langle S_{0,0}S_{0,n}\rangle^2=(1-z_1^2)^{2n}\det\begin{bmatrix}T_{RR}&T_{RL}\\T_{LR}&T_{LL}\end{bmatrix}, \tag{B9}$$

where the $n \times n$ matrices T_{IJ} are

$$T_{RR} = \begin{bmatrix} 0 & \cdots & A^{-1}(0;n-1)_{RR} \\ A^{-1}(1;0)_{RR} & \cdots & A^{-1}(1;n-1)_{RR} \\ \vdots & & \vdots \\ A^{-1}(n-1;0)_{RR} & \cdots & 0 \end{bmatrix}, \tag{B10}$$

$$T_{RL} = \begin{bmatrix} A^{-1}(0;1)_{RL}-c & \cdots & A^{-1}(0;n)_{RL} \\ A^{-1}(1;1)_{RL} & \cdots & A^{-1}(1;n)_{RL} \\ \vdots & & \vdots \\ A^{-1}(n-1;1)_{RL} & \cdots & A^{-1}(n-1;n)_{RL}-c \end{bmatrix}, \tag{B11}$$

$$T_{LR} = \begin{bmatrix} A^{-1}(1;0)_{LR}+c & \cdots & A^{-1}(1;n-1)_{LR} \\ A^{-1}(2;0)_{LR} & \cdots & A^{-1}(2;n-1)_{LR} \\ \vdots & & \vdots \\ A^{-1}(n;0)_{LR} & \cdots & A^{-1}(n;n-1)_{LR}+c \end{bmatrix}, \tag{B12}$$

$$T_{LL} = \begin{bmatrix} 0 & \cdots & A^{-1}(1;n)_{LL} \\ A^{-1}(2;1)_{LL} & \cdots & A^{-1}(2;n)_{LL} \\ \vdots & & \vdots \\ A^{-1}(n;1)_{LL} & \cdots & 0 \end{bmatrix} \tag{B13}$$

with $c = (z_1^{-1} - z_1)^{-1}$, $A^{-1}(k;k')_{IJ}$ $= (1/L)\sum_\theta e^{i\theta(k-k')}[B^{-1}(\theta)]_{IJ}$ and

$$[B^{-1}(\theta)]_{RR} = -[B^{-1}(\theta)]_{LL}$$

$$= \frac{1}{|1+z_1 e^{i\theta}|^2}\{[b_{22}^{-1}]_{UU} + [b_{22}^{-1}]_{DD}\}, \tag{B14}$$

$$[B^{-1}(\theta)]_{RL} = -[B^{-1}(\theta)]_{LR}^*$$

$$= \frac{-1}{(1+z_1 e^{-i\theta})}\left\{1 - \frac{1}{(1+z_1 e^{-i\theta})}([b_{22}^{-1}]_{UU}\right.$$

$$\left. -[b_{22}^{-1}]_{DD} - [b_{22}^{-1}]_{DU} + [b_{22}^{-1}]_{UD})\right\}, \tag{B15}$$

$$[b_{22}^{-1}]_{UU} = i\frac{v\bar{v}}{z_2}(1-\alpha^{-2(M_-+1)})\frac{v^2+\bar{v}^2\alpha^{-2M_+}}{v^2+\bar{v}^2\alpha^{-2M}}, \tag{B16}$$

$$[b_{22}^{-1}]_{DD} = -i\frac{v\bar{v}}{z_2}(1-\alpha^{-2(M_++1)})\frac{v^2+\bar{v}^2\alpha^{-2M_-}}{v^2+\bar{v}^2\alpha^{-2M}}, \tag{B17}$$

$$[b_{22}^{-1}]_{UD} = \frac{(v^2+\bar{v}^2\alpha^{-2M_+})(v^2+\bar{v}^2\alpha^{-2M_-})}{z_2\alpha(v^2+\bar{v}^2\alpha^{-2M_-})}, \tag{B18}$$

$$[b_{22}^{-1}]_{DU} = -[b_{22}^{-1}]_{UD}. \tag{B19}$$

If one were interested in the strip geometry ($L\to\infty$), then $T_{RR}=T_{LL}=0$ and $\langle S_{0,0}S_{0,n}\rangle$ could be written in terms of an $n \times n$ Toeplitz determinant.

---

[1] J.R. Schrieffer, *Theory of Superconductivity* (Addison-Wesley, New York, 1988).

[2] R.J. Bursill and C.J. Thompson, J. Phys. A **26**, 769 (1991).

[3] S.-Q. Shen and Z.-M. Qiu, Phys. Rev. Lett. **71**, 4238 (1993).

[4] M. Uehara, T. Nagata, J. Akimitsu, U. Takahashi, N. Mori, and K. Kinoshita, J. Phys. Soc. Jpn. **65**, 2764 (1996).

[5] P. Noziéres and S. Schmitt-Rink, J. Low Temp. Phys. **59**, 195 (1985).

[6] See, for example, R. Micnas, J. Ranninger, and S. Robaszkiewicz, Rev. Mod. Phys. **62**, 113 (1990).

[7] R.T. Scalettar, E.Y. Loh, Jr., J.E. Gubernatis, A. Moreo, S.R. White, D.J. Scalapino, R.L. Sugar, and E. Dagotto, Phys. Rev. Lett. **62**, 1407 (1989).

[8] E.H. Lieb and F.Y. Wu, Phys. Rev. Lett. **20**, 1445 (1968).

[9] N. Kawakami and S.-K. Yang, Phys. Rev. B **44**, 7844 (1991); J. Phys.: Condens. Matter **3**, 5983 (1991).

[10] N.D. Mermin and H. Wagner, Phys. Rev. Lett. **17**, 1133 (1966).

[11] E.H. Lieb, Phys. Rev. Lett. **62**, 1201 (1989).

[12] A. Auerbach, *Interacting Electrons and Quantum Magnetism* (Springer-Verlag, Heidelberg, 1994).

[13] See, for example, R.R.P. Singh and R.T. Scalettar, Phys. Rev. Lett. **24**, 3203 (1991).

[14] S.-Q. Shen and X.C. Xie, J. Phys.: Condens. Matter **8**, 4805 (1996).

[15] T. Momoi, Phys. Lett. A **201**, 261 (1995).

[16] S. Zhang, Phys. Rev. B **42**, 1012 (1990); G.-S. Tian, J. Phys. A **30**, 841 (1997).

[17] S. Zhang, J. Carlson, and J.E. Gubernatis, Phys. Rev. Lett. **74**, 3652 (1995); Phys. Rev. B **55**, 7464 (1997); J. Carlson, J.E. Gubernatis, G. Ortiz, and Shiwei Zhang, *ibid.* **59**, 12 788 (1999).

[18] M. Guerrero, G. Ortiz, and J.E. Gubernatis, Phys. Rev. B **59**, 1706 (1999).

[19] H. Yokoyama and H. Shiba, J. Phys. Soc. Jpn. **57**, 2482 (1988).

[20] S. White, Phys. Rev. Lett. **69**, 2863 (1992).

[21] F. Marsiglio, Phys. Rev. B **55**, 575 (1997); **60**, 3508(1999).

[22] K. Tanaka and F. Marsiglio, Phys. Lett. A **265**, 133 (2000).

[23] In the ground state all the electrons are in spin-paired (singlet) bound states which resemble Cooper pairs. These singlet pairs do not form bound states of pairs, that is, these pairs move freely throughout the chain. See K.-J.-B. Lee and P. Schlottmann, Phys. Rev. B **38**, 11 566 (1988).

[24] R.M. Noack, S.R. White, and D.J. Scalapino, Phys. Rev. Lett. **73**, 882 (1994).

[25] F. Marsiglio (private communication).

[26] B. Frischmuth, B. Ammon, and M. Troyer, Phys. Rev. B **54**, R3714 (1996).

[27] M. Greven, R.J. Birgeneau, and U.-J. Wiese, Phys. Rev. Lett. **77**, 1865 (1996).

[28] B. Ammon, M. Troyer, T.M. Rice, and N. Shibata, Phys. Rev. Lett. **82**, 3855 (1999).

[29] E. Dagotto and T.M. Rice, Science **271**, 618 (1996).

[30] T.M. Rice, Physica B **241-243**, 5 (1998).

[31] B. M. McCoy and T. T. Wu, *The Two-Dimensional Ising Model* (Harvard, Boston, 1973).

[32] J. G. Brankov, *Introduction to Finite-Size Scaling* (Leuven University Press, Leuven, 1996).

[33] N. Furukawa and M. Imada, J. Phys. Soc. Jpn. **61**, 3331 (1992).

[34] M. Guerrero, J.E. Gubernatis, and S. Zhang, Phys. Rev. B **57**, 11 980 (1998).

[35] P.A. Anderson, Phys. Rev. **112**, 1900 (1958).

[36] S. Zhang, J. Carlson, and J. E. Gubernatis, Phys. Rev. Lett. **78**, 4486 (1997).

[37] D. Bormann, T. Schneider, and M. Frick, Europhys. Lett. **14**, 101 (1991); Z. Phys. B: Condens. Matter **87**, 1 (1992).

[38] S.R. White, D.J. Scalapino, R.L. Sugar, N.E. Bickers, and R.T. Scalettar, Phys. Rev. B **39**, 839 (1989).

[39] E.Y. Loh, Jr. and D.K. Campbell, Synth. Met. **27**, A499 (1988); E.Y. Loh, Jr., J.T. Gammel, and D.K. Campbell, *ibid.* **57/2-3**, 4437 (1993).

[40] D. M. Ceperley (private communication).

[41] G. Ortiz, D.M. Ceperley, and R.M. Martin, Phys. Rev. Lett. **71**, 2777 (1993).

[42] G. Ortiz, J. Carlson, and J. E. Gubernatis (unpublished).